Systematic Molecular Engineering of a Series of Aniline-Based Squaraine Dyes and Their Structure-Related Properties

Taihong Liu,[†,‡] Xinglei Liu,[†] Weina Wang,[‡] Zhipu Luo,[§] Muqiong Liu,[||] Shengli Zou,[||] Cristina Sissa,[⊥] Anna Painelli,[⊥] Yuanwei Zhang,[†] Mikas Vengris,[#] Mykhailo V. Bondar,[¶] David J. Hagan,[▲] Eric W. Van Stryland,[▲] Yu Fang,[‡] and Kevin D. Belfield*[†,‡]

[†]Department of Chemistry and Environmental Science, College of Science and Liberal Arts, New Jersey Institute of Technology, 323 Martin Luther King, Jr. Blvd., Newark, New Jersey 07102, United States

[‡]School of Chemistry and Chemical Engineering, Shaanxi Normal University, Xi'an 710062, P. R. China

[§]Synchrotron Radiation Research Section, National Cancer Institute, Argonne National Laboratory, Argonne, Illinois 60439, United States

[||]Department of Chemistry, University of Central Florida, Orlando, Florida 32816, United States

[⊥]Department of Chemistry, Life Science and Environmental Sustainability, University of Parma, Parco Area delle Scienze 17/A, Parma 43124, Italy

[#]Light Conversion, Keramiku 2B, LT10233 Vilnius, Lithuania

[¶]Institute of Physics National Academy of Science of Ukraine, Prospect Nauki, 46, Kiev-28 03028, Ukraine

[▲]The College of Optics and Photonics (CREOL), University of Central Florida, P.O. Box 162700, Orlando, Florida 32816, United States

S *Supporting Information*
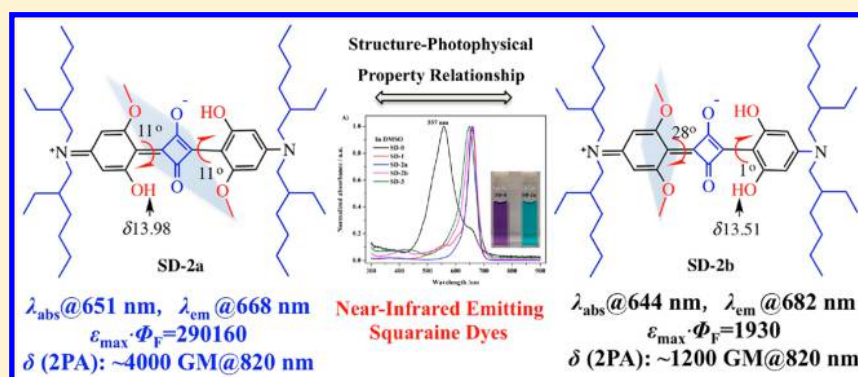
ABSTRACT: With the objective of developing new near-infrared fluorescent probes and understanding the effect molecular structure exerts on physical properties, a series of aniline-based squaraine dyes with different number and position of methoxy substituents adjacent to the squaraine core were synthesized and investigated. Using both computational and experimental methods, we found that the subtle changes of the number or position of the methoxy substituents influenced the twisting angle of the structure and led to significant variations in optical properties. Moreover, the methoxy substituent also affected aggregation behavior due to steric effects. The X-ray crystal structure of one of the key members of the series, **SD-2a**, clearly demonstrates the distortion between the four-membered squaraine core and the adjacent aniline ring due to methoxy substitution. Structure-related fast relaxation processes were investigated by femtosecond pump−probe experiments and transient absorption spectra. Quantum chemical calculations and essential state models were exploited to analyze the primary experimental results. The comprehensive investigation of structure-related properties of dihydroxylaniline-based squaraine dyes, with systematic substitution of OH by OCH_3 functional groups, serves as a guide for the design of novel squaraine dyes for photonics applications.

1. INTRODUCTION

Fluorescent dyes that absorb near-infrared (NIR) radiation have an increasing number of applications in materials science, biomedical science, and nanotechnology.[1−6] Squaraines, as a promising class of NIR dyes, have garnered attention in organic

Scheme 1. Synthesis of the Novel Squaraine Dyes[a]
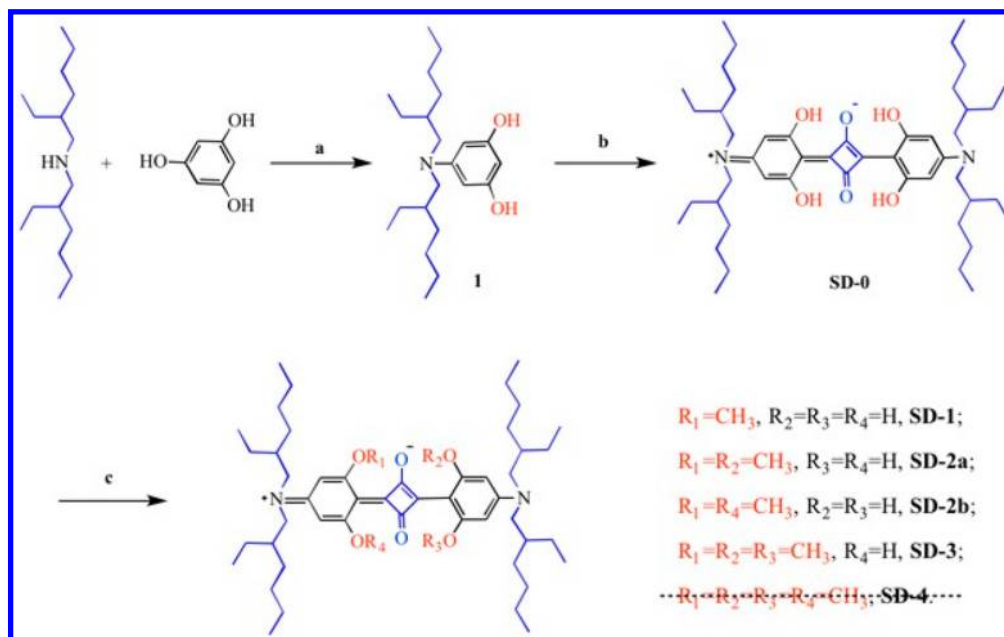
[a]Reaction conditions: (a) 1-butanol/toluene, Dean−Stark trap, reflux; (b) squaric acid, 1-butanol/toluene, Dean−Stark trap, reflux; (c) dimethyl sulfate, potassium *t*-butoxide, THF, rt.

solar cell materials,[7−10] optical storage media,[11−13] two-photon absorbing materials,[14,15] fluorescent probes,[16,17] and sensitizers for photodynamic cancer therapy.[18−20] Though significant attention has been paid to the design and synthesis of novel squaraine dyes, much less prevalent are systematic studies of structure-related photophysical properties of these promising photonic materials.[21]

Dihydroxylaniline-based squaraine derivatives with straight or branched terminal alkyl chains have been reported,[22−25] as have some relations between bulky terminal chains and intermolecular interactions and photophysical/photochemical properties.[24] In general, steric hindrance increases as the length of straight alkyl chains increases; meanwhile, branched alkyl chains such as isobutyl and 2-ethylhexyl have larger steric demands than straight-chain analogues. Chen et al. reported that both the terminal chains and the number of OH groups in the mono- or dihydroxylaniline-based squaraine dyes play important roles in determining aggregation behavior and photovoltaic performance.[25] Studies by Law showed that the electronic transitions of the squaraine dyes exhibited high sensitivity toward substitutional modifications and the surrounding solvent medium.[26] Thus, the impact of the molecular structure on intermolecular interactions as well as electronic and photophysical properties of squaraines can dramatically influence their behavior and potential applications, compelling us to further explore the fundamental structure-related properties of this important class of materials.

The OH group at the *ortho*-position in dihydroxylaniline-based squaraine dyes helps rigidify the squaraine core through intramolecular hydrogen bonding and increase stability.[27] We set out to study the influence of photophysical properties upon methodically replacing OH by OCH₃ moieties at a given position in the squaraine structure. In this work, 2,4-bis{4-[N,N-di(2-ethylhexyl)amino]-2,6-dihydroxyphenyl}squaraine (**SD-0**), a derivative with four OH moieties, all *ortho* to the squaraine ring, was synthesized first, followed by reaction with

dimethyl sulfate in the presence of potassium *tert*-butoxide in varying stoichiometries to prepare a series of novel methoxy-containing squaraine derivatives with two and three methoxy groups (it was not possible to isolate the tetramethoxy derivative) as depicted in Scheme 1. The effects of steric hindrance evoked by the presence of methoxy groups and disruption of intramolecular hydrogen bonding on the optical properties and resulting aggregation behavior of the dyes were examined experimentally and theoretically. Fast relaxation processes in the excited electronic states and two-photon absorption (2PA) spectra of the new squaraines were also investigated to further understand excited state dynamics and behavior.

2. EXPERIMENTAL SECTION

2.1. Crystal Structure Determination. Single-crystal X-ray diffraction data were collected at ChemMatCARS (Sector 15-ID-D) of the Advanced Photon Source, Argonne National Laboratory, USA. The crystals were mounted on a nylon loop with glycerol and cooled to 100 K with an Oxford Cryojet. The beam energy was 30 keV. Data were collected using a Bruker D8 fixed-chi diffractometer equipped with a Pilatus 3R 1 M detector. Data were processed with APEX2 suite software.[28] The structure was solved by SHELXT[29] and refined by SHELXL.[30] The four-membered core was unstrained during refinement, while the branched alkyl chains were restrained with proper bond length. Non-hydrogen atoms were refined with anisotropic displacement parameters, and hydrogen atoms on carbons were placed in idealized positions. OLEX2[31] and COOT[32] software programs were used for modeling the disordered conformations. Crystals of **SD-2a** were grown using vapor diffusion with saturated DMSO solution. The crystallographic summary is listed in Supporting Information Tables S1−S4.

2.2. Transient Absorption Pump−Probe Measurements. Femtosecond transient absorption spectra were

Chart 1. Zwitterionic Structures, Partial Assignment of the Proton NMR, and Key Dihedral Angles of SD-0 and Its Derivatives Calculated at the B3LYP/6-31G(d) Level
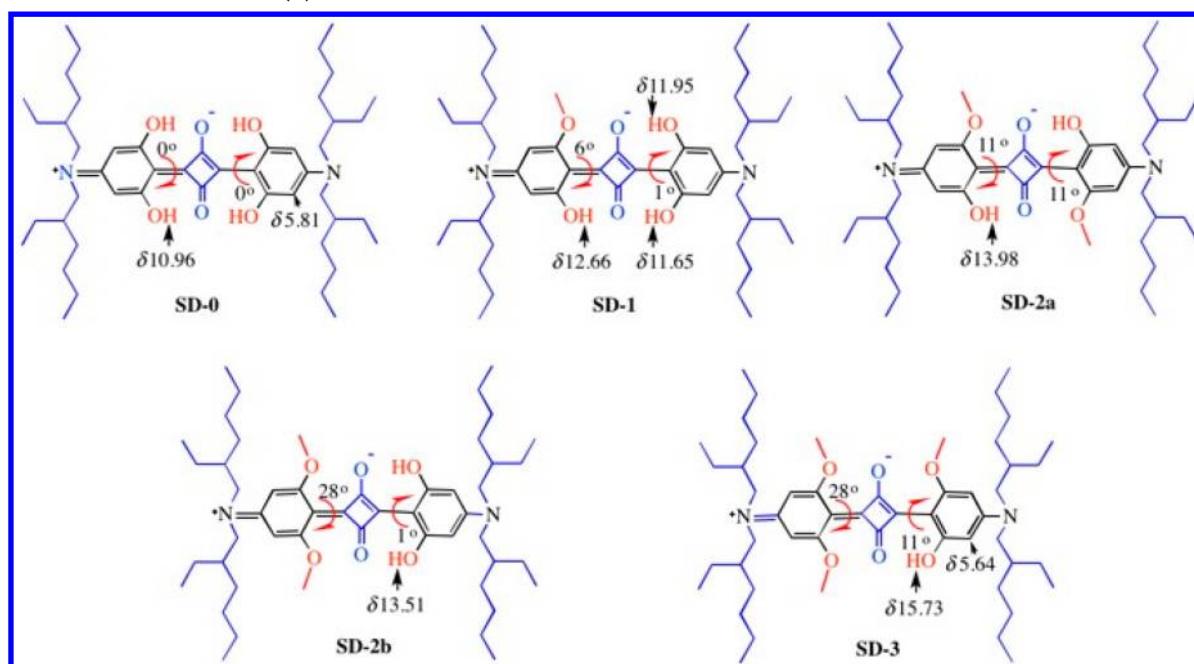
recorded on a commercial transient absorption spectrometer Harpia (Light Conversion), built following a design described in detail previously.[33,34] In short, the pump and probe pulses are derived from an amplified Yb:KGW laser (Pharos, Light Conversion), providing 90 μJ pulses with the central wavelength of 1030 nm at a 66 kHz repetition rate. An optical parametric amplifier (Orpheus, Light Conversion) was used to obtain tunable pump pulses at 650 nm, while a white light continuum, generated in a sapphire window from the fundamental output of the laser, was used to probe absorption changes in the 450−950 nm range. A mechanical chopper (MC2000, Thorlabs) alternately blocked and unblocked the pump beam, the state of which (on or off) was monitored by a photodiode (Thorlabs DET10A/M). The squaraine dyes were dissolved in dichloromethane (DCM) at concentrations resulting in ~15−35% transmission through the cell with an optical path length of 1 mm. The transmittance spectra were recorded and binned according to the state of the chopper during each spectrum. Average pumped and dark spectra were obtained, from which the absorption change was calculated. A Berek polarization compensator (Newport 5540M) was used to set the polarization of the pump beam at the magic angle (54.7°) with respect to the probe in order to avoid signals due to rotational diffusion of the sample molecules. The excitation pulse energy used in the experiments was 4.5 nJ; the probe beam diameter at the sample spot was ca. 90 μm (full width at half-maximum, fwhm); and the pump diameter was ~300 μm. The time resolution (fwhm) of the instrument response function was ~240 fs.

2.3. Two-Photon Absorption (2PA) Measurements. Degenerate 2PA spectra of the new squaraines were obtained with a 1 kHz femtosecond laser system (Ti:sapphire regenerative amplifier (Legend Duo⁺) pumping an OPA (HE-TOPAS), all from Coherent, Inc.) using the open-aperture Z-scan technique.[35] All measurements were performed in 1 mm quartz cells with dye concentrations ~10^{-3} M. The

experimental Z-scan setup was calibrated with ZnSe, CdSe, and SiO₂ as standards.

2.4. Synthesis of the Parent Dye SD-0. According to the previously published procedures,[24,25] the key intermediate **1** was prepared in a yield of 52% by reacting phloroglucinol with bis(2-ethylhexyl)amine. Condensation of **1** with squaric acid gave the parent dye **SD-0** as dark blue viscous oil in 24% yield. $R_f \approx 0.67$ (*n*-hexane/ethyl acetate, 9/1, v/v). ¹H NMR (CDCl₃, 500 MHz, ppm): δ 10.96 (s, 4 H, phenol-*H*), 5.81 (s, 4 H), 3.32−3.28 (m, 8 H), 1.85−1.81 (m, 4 H), 1.35−1.24 (m, 32 H), 0.92−0.88 (m, 24 H). ¹³C NMR (CDCl₃, 126 MHz, ppm): δ (squaraine core) 181.36, 162.50, (anilinyl) 161.07, 158.27, 102.46, 94.46, 56.59 (−NCH₂−), 38.12, 30.45, 28.50, 23.81, 23.09, 14.04, 10.63. HR-MS (*m/z*): [M + H]⁺ Calculated for C₄₈H₇₇N₂O₆, 777.5776; Found, 777.5789.

2.5. General Procedures for the Synthesis of Novel Squaraine Derivatives. Reagents and general conditions for the synthesis of the squaraine dyes are presented in Scheme 1. Compound **SD-0**, potassium *tert*-butoxide, and dry THF were placed in a round-bottom flask, which was then flushed with N₂. Dimethyl sulfate in THF was added, and the solution was stirred at room temperature for 8 h. The resulting residue was concentrated, dissolved in DCM, washed with water, then dried over anhydrous MgSO₄. After filtering and removal of the solvent *in vacuo*, the crude product was purified by column chromatography with *n*-hexane/ethyl acetate as eluent, affording the corresponding methyl-substituted squaraine derivatives. We note that several of the desired compounds could be generated in the one-pot reaction and isolated, while their yields depended on the stoichiometry of starting material **SD-0**, dimethyl sulfate, and the base added to the reaction system. The overall yields of the derivatives were in the range of 60−70%, and structures of all dyes were fully confirmed using standard characterization methods.

SD-1: blue viscous oil. $R_f \approx 0.43$ (*n*-hexane/ethyl acetate, 9/1, v/v). ¹H NMR (CDCl₃, 500 MHz, ppm): δ 12.66 (1 H, phenol-*H*), 11.95 (1 H, phenol-*H*), 11.65 (1 H, phenol-*H*),
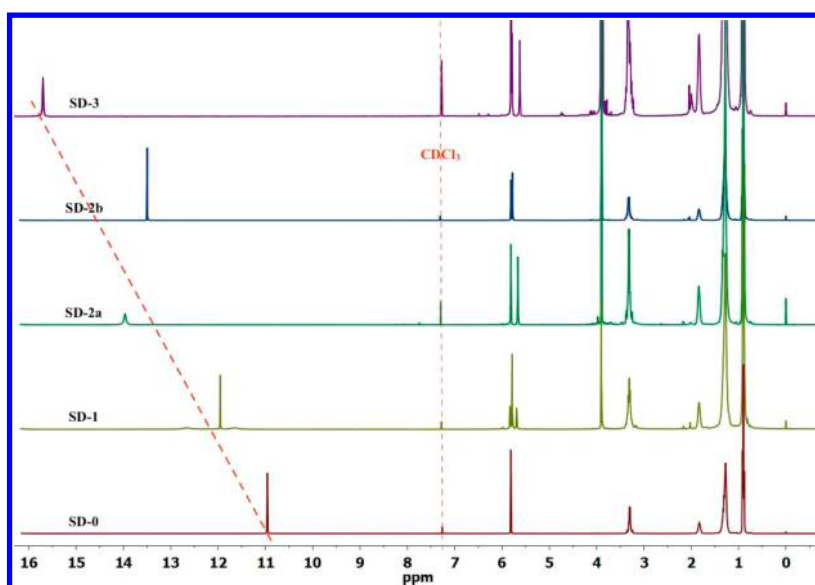
Figure 1. Overlay of ^{1}H NMR spectra of squaraines **SD-0**, **SD-1**, **SD-2a**, **SD-2b**, and **SD-3** in CDCl$_3$.

5.84 (1 H), 5.80 (2 H), 5.70 (1 H), 3.91 (3 H, CH_3), 3.37–3.27 (8 H), 1.86–1.82 (4 H), 1.40–1.24 (32 H), 0.97–0.89 (24 H). ^{13}C NMR (CDCl$_3$, 126 MHz, ppm): δ 168.88, 163.83, 163.80, 162.92, 158.72, 156.56, 104.00, 102.14, 94.81, 94.26, 88.78, 56.68 (−NCH_2−), 56.53 (−NCH_2−), 55.45 (−OCH_3), 38.12, 30.65, 28.48, 23.78, 23.09, 14.03, 10.61. HR-MS (*m/z*): [M + H]$^+$ Calculated for C$_{49}$H$_{79}$N$_2$O$_6$, 791.5933; Found, 791.5939.

SD-2a: green solid. R_f ≈ 0.57 (*n*-hexane/ethyl acetate, 4/1, v/v). ^{1}H NMR (CDCl$_3$, 500 MHz, ppm): δ 13.98 (2 H, phenol-*H*), 5.83 (2 H), 5.67 (2 H), 3.91 (6 H, CH_3), 3.38–3.27 (8 H), 1.88–1.83 (4 H), 1.41–1.24 (32 H), 0.99–0.90 (24 H). ^{13}C NMR (CDCl$_3$, 126 MHz, ppm): δ (squaraine core) 182.10, 171.71, (anilinyl) 165.83, 163.02, 156.88, 103.42, 94.82, 88.60, 56.64 (−NCH_2−), 55.45 (−OCH_3), 38.08, 30.64, 28.67, 23.94, 23.10, 14.04, 10.74. HR-MS (*m/z*): [M + H]$^+$ Calculated for C$_{50}$H$_{81}$N$_2$O$_6$, 805.6089; Found, 805.6078.

SD-2b: blue solid. R_f ≈ 0.69 (*n*-hexane/ethyl acetate, 4/1, v/v). ^{1}H NMR (CDCl$_3$, 500 MHz, ppm): δ 13.51 (2 H, phenol-*H*), 5.82 (2 H), 5.79 (2 H), 3.91 (6 H, CH_3), 3.40–3.27 (8 H), 1.88–1.83 (4 H), 1.40–1.24 (32 H), 0.98–0.88 (24 H). ^{13}C NMR (CDCl$_3$, 126 MHz, ppm): δ (squaraine core) 182.84, 180.15, 165.29, (anilinyl) 163.97, 161.80, 160.50, 153.78, 107.07, 99.62, 94.28, 89.15, 56.93 (−NCH_2−), 56.71 (−NCH_2−), 55.69 (−OCH_3), 38.28, 37.77, 30.96, 30.41, 28.47, 23.77, 23.10, 14.04, 10.94, 10.61. HR-MS (*m/z*): [M + H]$^+$ Calculated for C$_{50}$H$_{81}$N$_2$O$_6$, 805.6089; Found, 805.6087.

SD-3: blue solid. R_f ≈ 0.69 (*n*-hexane/ethyl acetate, 1/1, v/v). ^{1}H NMR (CDCl$_3$, 500 MHz, ppm): δ 15.73 (1 H, phenol-*H*), 5.83–5.80 (3 H), 5.64 (1 H), 3.93 (3 H, CH_3), 3.90 (6 H, CH_3), 3.39–3.31 (8 H), 1.87–1.83 (4 H), 1.37–1.24 (32 H), 0.94–0.90 (24 H). ^{13}C NMR (CDCl$_3$, 126 MHz, ppm): δ (squaraine core) 188.44, 185.19, 177.21, 173.87, (anilinyl) 168.54, 164.24, 161.61, 158.98, 153.42, 106.75, 99.94, 94.91, 89.28, 88.70, 56.92 (−NCH_2−), 56.82 (−NCH_2−), 55.77 (−OCH_3), 55.44 (−OCH_3), 38.30, 37.69, 30.96, 30.91, 30.61, 28.97, 28.94, 28.64, 24.19, 24.16, 23.92, 23.11, 23.05, 14.05, 14.02, 10.93, 10.90, 10.73. HR-MS (*m/z*): [M + H]$^+$ Calculated for C$_{51}$H$_{83}$N$_2$O$_6$, 819.6246; Found, 819.6226.

3. RESULTS AND DISSCUSSION

3.1. Synthesis and Characterization. As illustrated in Scheme 1 and Chart 1, a series of methyl-substituted squaraine derivatives **SD-1**, **SD-2a**, **SD-2b**, and **SD-3** were prepared via nucleophilic substitution reactions. **SD-0** with four OH groups serves as both the parent compound and control.[36,37] The subsitution of one hydroxy H provided the monomethylated derivative **SD-1**. Interestingly, substitution of two hydroxy H's of **SD-0** produced two distinct dimethylated isomers **SD-2a** and **SD-2b**, with two methyl groups on different or the same aniline moiety, respectively. Likewise, substitution of three hydroxy H's of **SD-0** generated trisubstituted squaraine **SD-3**. As indicated, the tetramethylated derivative **SD-4** was not attained under either the same reaction conditions or an alternate route by reaction of *N,N*-bis(2-ethylhexyl)-3,5-dimethoxyaniline with squaric acid (cf. Scheme S1). To this we ascribe strong steric forces evoked by the introduction of four methoxy groups *ortho* to the central squaraine core that would eliminate all intramolecular hydrogen bonding and impose severe intramolecular steric effects.

NMR data were helpful in confirming the structure of the dyes. As shown in Figure 1 and Chart 1, the complete proton spectrum for each dye can be reasonably assigned. In detail, the protons of the benzene ring in **SD-0** appeared as a singlet at δ 5.81 ppm, and the OH protons appeared at δ 10.96 ppm. Upon methylation, the OH proton at the *ortho*-position of the aniline experienced a large shift downfield compared with parent **SD-0** (Δδ = 3.02 ppm for **SD-2a**, 2.55 ppm for **SD-2b**, and 4.77 ppm for **SD-3**). The proton signals at the *ortho*-position relative to N of the aniline ring show clear translocation, with one shifted upfield from 5.81 ppm in **SD-0** to 5.64 ppm in **SD-3**. This means that the introduction of the methyl group exerts a significant influence on the effective conjugation and the intramolecular hydrogen bonding between OH and the squaryl oxygen in this series of dyes.[38,39] It is worth noting that for asymmetrical dye **SD-1** its three phenol protons show more than one signal (cf. Figure S6), not as sharp as other squaraine derivatives; moreover, the carbon signals of the squaraine core of **SD-1** were not normally observed in the range of 170−190 ppm (cf. Figure S7) and are related to the changes of the π-
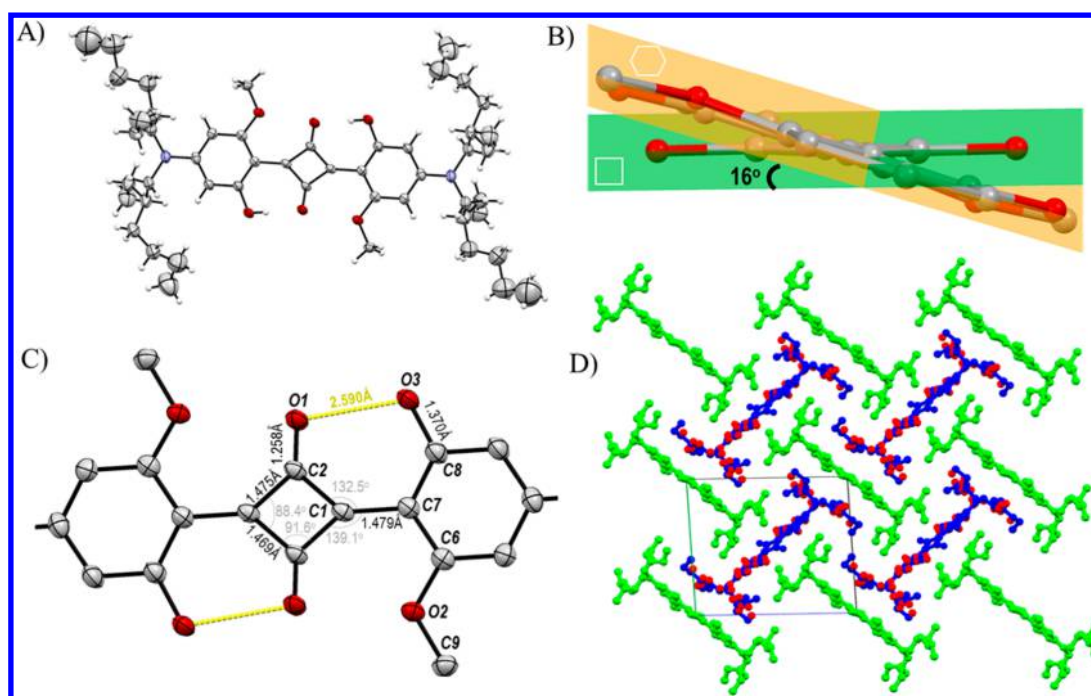
Figure 2. Crystal structure and packing of **SD-2a**. (A) Crystal structure of **SD-2a** is shown with ORTEP diagrams with thermal ellipsoid at the 20% level. Atom color scheme: C: gray; O, red; N, blue; H, white. (B) The crystal structure of **SD-2a** shows distortion of a four-carbon core plane (green) away from the plane of the phenol moiety (orange). (C) The bond lengths and angles of the four-carbon core are also labeled. The hydrogen bonds between carbonyl groups of the four-carbon core and hydroxyl groups of phenol are shown as yellow dash. (D) The crystal packing of **SD-2a**. The nonequivalent molecules are shown in different color including the disordered parts.

Table 1. Photophysical Properties of the SD Dye Series

dyes	λ_{abs}^{a} [nm]	λ_{em}^{a} [nm]	ε^{a} [10^5 M^{-1}·cm^{-1}]	$\Delta\lambda^{a}$ [nm/cm^{-1}]	fwhm^{a} [nm]	τ_F^{a} [ns]	Eg$_{expl.}^{b}$ [eV]	LUMO^{c}[eV]	HOMO^{c} [eV]	ΔE_{H-L}^{d} [eV]	Φ_F^{e}	$(\Phi_{ph}\cdot10^8)^{a}$
SD-0	657	670	2.95	13/300	33	2.39	1.84	−2.53	−4.94	2.41	0.77	6.1
SD-1	652	668	2.71	16/370	33	1.49	1.85	−2.31	−4.73	2.42	0.41	1.7
SD-2a	651	668	2.82	17/390	41	2.32	1.85	−2.12	−4.52	2.40	0.72	7.8
SD-2b	644	682	1.93	38/865	63	∼0.10	1.86	−2.13	−4.59	2.46	0.01	0.4
SD-3	639	690	1.16	51/1157	77	∼0.10	1.87	−1.93	−4.36	2.43	0.01	4.1
SD-4	/	/	/	/	/	/	/	−1.80	−3.98	2.18	/	/

^{a}Measured in DCM. ^{b}Optical band gap (Eg$_{expl.}$) = 1240/λ onset from UV−vis spectra. ^{c}Calculated by B3LYP/6-31G(d). $^d\Delta E_{H-L}$ = LUMO−HOMO. ^{e}Error limit ±5%.

conjugation of the molecular backbone consistent with prior reports.[40,41] It was observed that the intramolecular non-covalent interaction in this series plays an important role in the charge delocalization and the rigidity of the planarity of the zwitterionic structure. Similar experimental phenomena and the presence of the conformational isomers were reported by Yang and co-workers based on variable-temperature NMR data,[42] while the presence of conformational isomers on hydroxy squaraines was reported by Kazmaier.[40] As Lin et al. reported,[41] the NMR spectra of an unsymmetrical hydroxyl squaraine derivative also support the existence of conformation isomers, creating additional resonances in the spectrum, consistent with our observations. Thus, the preferred charge delocalization between the zwitterionic donor−acceptor−donor structure and molecular planarity in asymmetrical squaraines and dominance of conformational isomers should be different from the symmetrical analogues.[43] The structural isomers **SD-2a** and **SD-2b** were identified by ^{1}H NMR, ^{13}C NMR, and X-ray crystallography (cf. Figure S1). In the ^{13}C NMR spectrum of **SD-2a** eight signals for the chemically inequivalent carbons in aromatic and squarainyl moieties were evident above δ 77.0

ppm, while 11 were observed for **SD-2b**, in agreement with theoretical predictions, further confirming their structures.

3.2. Crystal Structure of Dye SD-2a. The crystal structure was solved in the centrosymmetric triclinic space group with two half nonequivalent molecules in the asymmetry unit (Figure 2A). One of them is disordered in the crystal. The end-branched alkyl chains are flexibly demonstrated by their large ellipsoid radius. The plane of the four-membered squaraine core is distorted by 16° away from the plane of phenol ring due to steric effects of the methoxy group on the aromatic ring (Figure 2B). The squaryl carbonyl is involved in hydrogen bonding with the nearby hydroxy group of the aromatic ring at a distance of 2.590 Å, which is slightly shorter compared to the value in **SD-0** (2.642 Å).[44] Hydrogen bonding along with the steric hindrance imposed by the methoxy group results in distortion of the squaraine core with bond lengths of 1.475 and 1.469 Å and inner bond angles 88.4 ° and 91.6 ° (Figure 2C). The **SD-2a** molecules are compactly packed in the crystal cell with the terminal alkyl chain oriented toward the conjugated π system (Figure 2D).
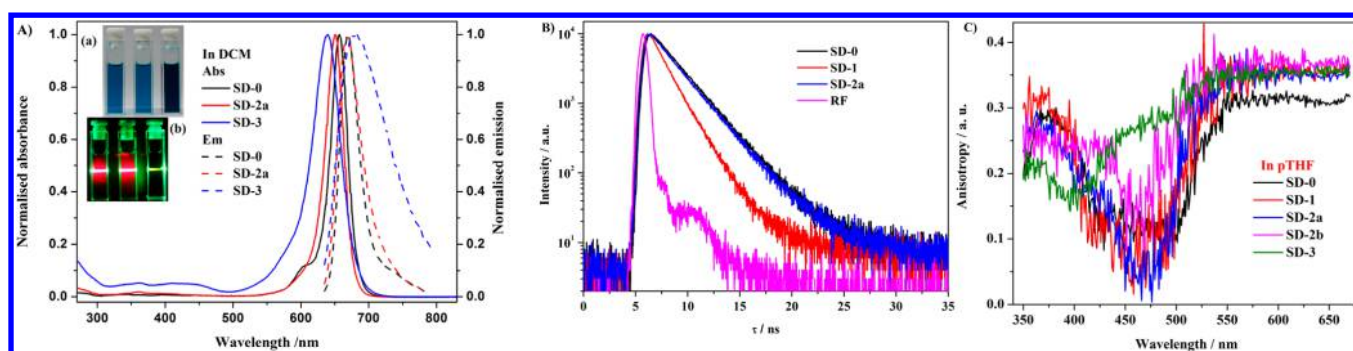
Figure 3. (A) Normalized absorption and fluorescence spectra of **SD-0**, **SD-2a**, and **SD-3** in DCM. Inset: images of these dyes in DCM under visible light (a) and laser beam (λ = 520−540 nm, from left to right: **SD-0**, **SD-2a**, and **SD-3**) (b). (B) Fluorescence decay curves of **SD-0**, **SD-1**, and **SD-2a** in DCM with instrument response function (RF). (C) Excitation anisotropy of the dyes in pTHF.
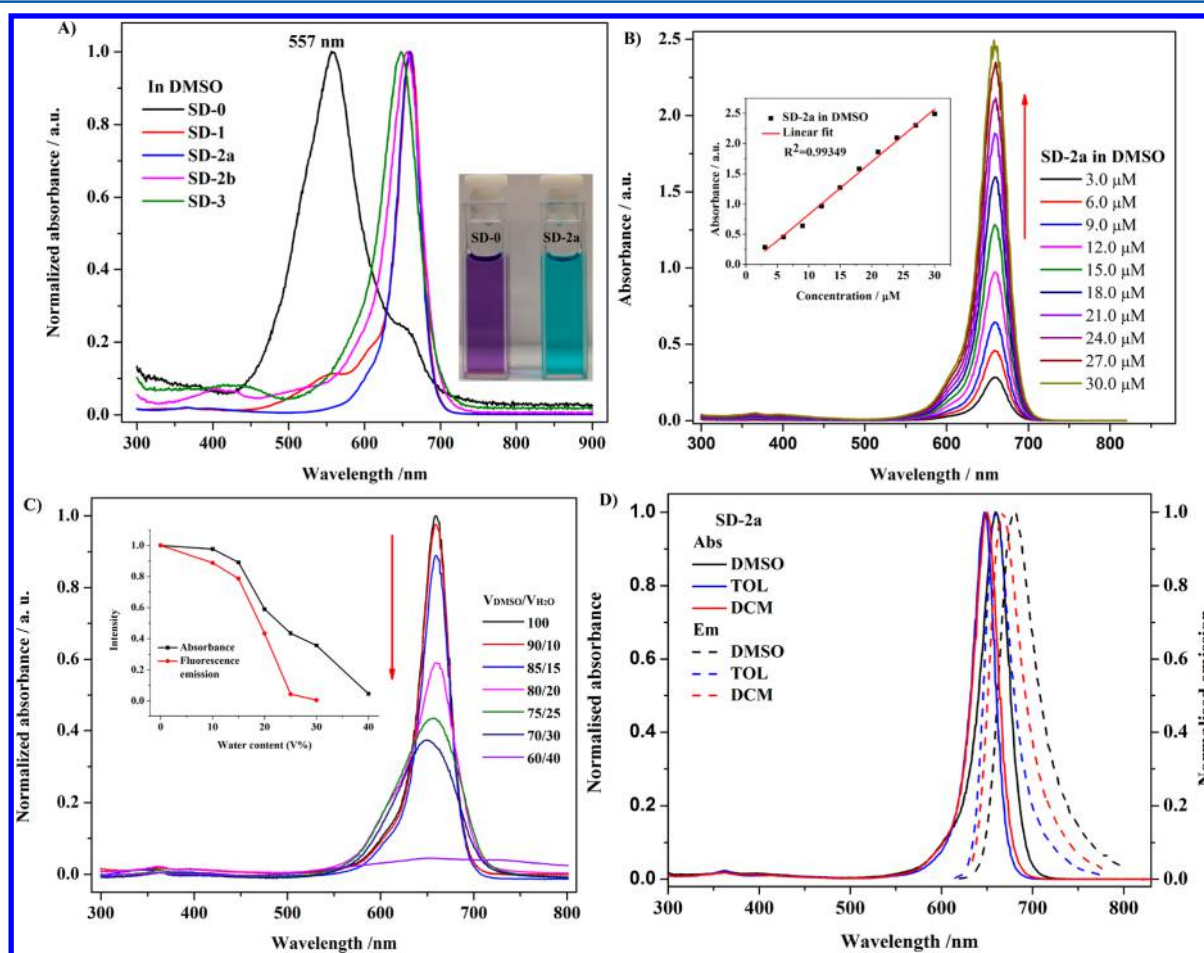
Figure 4. (A) Normailzed absorption of **SD-0** and four squaraine derivatives in DMSO. Inset: images of **SD-0** and **SD-2a** in DMSO under visible light. (B) Absorption spectra of **SD-2a** in DMSO at different concentrations. Inset: plots of absorption intensity at 660 nm to the concentration of **SD-2a**. (C) Absorbance of **SD-2a** in the mixture of DMSO and water with different ratio. Inset: plots of the normalized absorbance and fluorescence intensity to the water content in the DMSO/H$_2$O mixture (v/v). (D) Normalized absorption and fluorescence spectra of **SD-2a** in different solvents.

3.3. Spectral Properties. The optical properties of **SD-0** and four methylated derivatives (**SD-1**, **SD-2a**, **SD-2b**, and **SD-3**) were investigated in DCM in order to evaluate the effect of the structural modification and are summarized in Table 1. Typical absorption and emission spectra of **SD-0**, **SD-2a**, and **SD-3** are presented as examples in Figure 3A. As depicted, all the derivatives have sharp and intense absorption in the long-wavelength region, similar to the parent dye **SD-0**. In particular, **SD-2a** has a sharp absorption peak at 651 nm and a strong fluorescence emission maximum at 668 nm as well as a

characteristically small Stokes shift in DCM. A weak vibronic shoulder at 605 nm was found only in the absorption spectrum of **SD-0**.[45−47] The absorption maxima of **SD-2b** and **SD-3** show hypsochromic shifts of 13 and 18 nm, respectively, relative to **SD-0**.

The respective molar extinction coefficients of the squaraine series are in the range of $(1.1−2.8) \times 10^5$ M^{-1}·cm^{-1}, the same order of magnitude as **SD-0**. The fluorescence spectra undergo a slight bathochromic shift and marked broadening as the number of methoxy groups increases. The fwhm values of the

fluorescence emission increased from 33 nm of **SD-1** to 77 nm of **SD-3**. Their fluorescence quantum yield, Φ_F, values follow the order of **SD-0** > **SD-2a** > **SD-1** ≫ **SD-2b** ≈ **SD-3**. Among the methylated derivatives (in DCM), **SD-2a** afforded a higher Φ_F value (0.72), while the Φ_F values of **SD-2b** and **SD-3** were found to be very low (around 0.01). The suppression of Φ_F after attaching different methyl groups likely arises from intramolecular rotation of the substituent groups, which provides additional channels for nonradiative de-excitation.[15] The same order was observed for fluorescence lifetimes, which corresponded to a single exponential decay, e.g., 1.49 ns for **SD-1** and 2.32 ns for **SD-2a** (Figure 3B), while the fluorescence lifetimes of **SD-2b** and **SD-3** were found to be very short (~0.1 ns). With respect to the optical properties, a comparison of **SD-2a** and **SD-2b** revealed differences caused by the position of methyl substitution. The results suggest a large decrease in efficient delocalization throughout the conjugated backbone of **SD-2b**, a supposition further supported by computational results discussed below.

Excitation anisotropy spectra provided information regarding the nature of linear absorption bands. The excitation anisotropy spectra of the dyes in viscous polytetrahydrofuran (pTHF) are presented in Figure 3C. We can see that the values of anisotropy were nearly constant in the main long-wavelength absorption band[48] and reached their maximum value $r \approx r_0 \approx 0.37$ for the modified dyes, and the value of **SD-0** is around 0.31, reflecting a nearly parallel orientation of the absorption and the emission transition dipoles of new dyes in this spectral range. At higher energy, the anisotropy decreased and dips were observed near 470 nm for **SD-0**, **SD-1**, **SD-2a**, and **SD-2b** and 400 nm for **SD-3**, respectively, which suggests an additional electronic state with a transition dipole noncollinear with the main absorption band.[49] The photodecomposition quantum yields (Φ_{ph}) of the dyes in DCM were calculated in the range of $(0.4-7.8) \times 10^{-8}$, indicating very good photostability of the squaraine derivatives with substantial promise as probes for bioimaging.

3.4. Aggregation Studies. Squaraine dyes are known for their tendency to aggregate in different environments. Aggregate spectra are characterized by the appearance of new absorption bands and/or broadened spectra and sometimes by the quenching of the fluorescence intensity.[22−25] Figure 4A shows absorption spectra measured for the squaraine dyes in DMSO at the nominal concentration of ~5.0×10^{-6} M. The absorption spectrum of **SD-0** shows a clear signature of aggregation: the small peak at 655 nm is clearly the monomer band, but the large peak at 557 can be safely ascribed to an H-aggregate. The solution color of **SD-0** in DMSO is purple, and the dye existed mainly in its aggregated form. This is partially due to the fact that the end branch of bis(2-ethylhexane) may not efficiently prevent aggregation in poor solvents. In DMSO solution, **SD-2a** appeared as the typical blue color. All four derivatives showed characteristically sharp and intense absorption bands centered around 650 nm in DMSO that are indicative of the presence of mostly monomeric, i.e., non-aggregated, squaraine dyes.[46,50] The absorption spectra of **SD-2a** in DMSO with various concentrations are given in Figure 4B. **SD-2a** exhibited a well-defined absorption band with a maximum at 660 nm. No changes in the spectral bands were observed with increasing **SD-2a** concentration, thus indicating the dye's ability to remain in monomeric form even at relatively higher concentrations.

Meanwhile, the optical intensity and fluorescence emission of **SD-2a** at the same concentration level in the DMSO/H$_2$O mixture (Figure 4C) were also measured. With an increase in the water content in the mixture from 0 to 40%, **SD-2a** revealed no spectral broadening or aggregation-induced shoulder in the absorption spectra. Both the absorption intensity and fluorescence emission intensity decreased with increasing H$_2$O concentration, with fluorescence decreasing faster and not producing any new spectral peak. The results demonstrated that the modified squaraines appear unable to get close enough to interact with each other because of the steric effect introduced by the methoxy groups.

3.5. Solvent Effect. In an effort to gain further insight into the photophysical properties of the series of dyes, the absorption and emission behavior of the squaraines in toluene (TOL), tetrahydrofuran (THF), acetontrile (ACN), and dimethyl sulfoxide (DMSO) were conducted, and the corresponding photophysical data are summarized in Table 2. Typical absorption and emission spectra of **SD-2a**, as an example in DCM, TOL, and DMSO, are presented in Figure 4D. The steady-state absorption maximum and the fluorescence emission maximum and the fluorescence emission are weakly affected by the solvent. While in general a slight red-shift was observed with increasing solvent polarity, the behavior is nonmonotonic, suggesting the possibility of site-specific effects, most probably related to the presence of pH-sensitive groups in the squaraine systems. The fluorescence quantum yields and fluorescence lifetimes decreased from nonpolar to polar media. In the case of **SD-2a**, the results show that the fluorescence quantum yield can be observed to be relatively high in nonpolar solvents ($\Phi_F = 0.81$ in TOL) and low in polar solvents ($\Phi_F = 0.38$ in DMSO). Finally, a very interesting result comes from the analysis of the Φ_F values and fluorescence lifetimes of **SD-3** in different solvents. The Φ_F values decreased dramatically from 0.30 in TOL to 0.02 in THF and 0.01 in DMSO (Table 2). This phenomenon was confirmed by the Φ_F difference in cyclohexane (0.30) and dioxane (0.04). We can conclude that the involvement of a nonradiative channel is very sensitive to the rapid excited-state charge transfer or electronic redistribution in squaraines, and the polarity of the solvent favors the shortening of the fluorescence lifetimes by forming the solute−solvent complexes.[26]

3.6. Transient Absorption Spectroscopy and 2PA Spectra of New Squaraine Derivatives. The nature of transient absorption processes in **SD-0**−**SD-3** was investigated in DCM solution by femtosecond pump−probe experimental methodology.[33,34] The contour plots of the induced optical density signals, ΔD, time-resolved transient absorption spectra, where ΔD is a function of τ_D ($\Delta D = f(\tau_D)$ and τ_D is the time delay between pump and probe pulses), of the new squaraine dyes were obtained under their excitation in the main absorption bands ($\lambda_{ex} \approx 650$ nm) and presented in Figure 5. In general, the nature of the transient absorption spectra can be attributed to excited state absorption (ESA), saturable absorption (SA), and gain processes.[51] The first (positive) transient absorption contours at ~500 nm (Figure 5B) are typical ESA bands for similar squaraine-type structures with the maxima absorption wavelengths in the spectral range 630−660 nm.[52] The second (negative) transient absorption contours, with maximum at ~650 nm, are a combination of SA and gain signals with the dominant role of SA in the spectral range ~550−660 nm and gain processes for $\lambda > 680$ nm. Relatively narrow negative contours for **SD-0** and **SD-1** (Figures 5B$_1$ and

Table 2. Photophysical Properties of the Dyes in Different Solvents

dyes	SD-1				SD-2a				SD-2b				SD-3			
solvents	TOL	THF	ACN	DMSO	TOL	THF	ACN	DMSO	TOL	THF	ACN	DMSO	TOL	THF	ACN	DMSO
λ_{abs} [nm]	647	650	650	660	646	647	648	660	630	636	643	656	630	631	638	648
λ_{em} [nm]	660	664	667	680	659	662	667	680	660	671	688	680	689	694	686	697
ε_{max} [10^5 M^{-1}·cm^{-1}]	2.59	2.44	2.58	1.05	2.53	2.50	2.34	2.04	1.53	1.73	1.61	1.41	1.09	1.11	0.98	1.17
$\Delta\lambda$ [nm]	13	14	17	20	13	15	19	20	30	35	43	45	59	63	48	49
$\Delta\tilde{\nu}$ [cm^{-1}]	300	320	390	450	300	350	440	450	721	820	1017	938	1359	1439	1097	1085
τ_F [ns]	0.75	1.05	0.73	0.81	2.26	1.92	1.38	1.64	0.15	0.12	---	---	1.22	0.17	---	---
Φ_F	0.25	0.34	0.23	0.14	0.81	0.64	0.40	0.38	0.01	0.01	---	0.01	0.30	0.02	---	0.01

5B$_2$) and increased spectral width for **SD-2b** and **SD-3** (Figures 5B$_3$ and 5B$_4$) were in good agreement with the corresponding steady-state spectral data in Table 1 and Figure 3A. The global fit of the experimental data (Figure 5A) gives several exponential components in the obtained kinetic curves $\Delta D = f(\tau_D)$. The short-wavelength ESA bands at ~500 nm arise in the first ~500 fs (Figure 5C) and then slowly relax to zero with characteristic times of ≈2.6 ns (**SD-0**), ≈2.0 ns (**SD-1**), ≈2.6 ns (**SD-2a**), ≈51 ps (**SD-2b**), and ≈46 ps (**SD-3**). In the spectral range of the maximum negative transient absorption signals (~650−660 nm) kinetic curves exhibit two main relaxation processes with characteristic times ~1−3 ps and ~2−3 ns (for **SD-0**, **SD-1**, **SD-2a**) or ~50−70 ps (for **SD-2b**, **SD-3**). The short relaxation time can be attributed to solvate relaxation processes in low viscosity dye solution.[53] The second relatively long characteristic time obviously is related to the electronic deactivation S$_1$ → S$_0$. Relatively high fluorescence quantum yields ($\Phi_F \sim 0.4-0.8$) and efficient gain processes in **SD-0**, **SD-1**, and **SD-2a** (Figure 5B) suggest the potential for their superluminescence application.[51,54]

The degenerate 2PA spectra of **SD-2a** and **SD-2b** were obtained over a broad spectral range by the open-aperture Z-scan technique and presented in Figure 6. The shape of these spectra is similar to known symmetrical squaraine derivatives with maximum linear absorption wavelengths at ~600−700 nm.[54,55] Absolute cross section values up to ~4000 GM were observed for the symmetrical squaraine **SD-2a** in the short wavelength two-photon allowed absorption range, in line with the typically large 2PA cross sections observed for squaraine dyes, also due to preresonance enhancement.[56] At long wavelengths, one-photon allowed 2PA efficiency decreased dramatically due to the selection rules for electronic dipole transitions. The small peak observed at ~1100 nm corresponds to a state located at 550 nm, almost 3000 cm^{-1} higher in energy than the one-photon state. Accordingly it is difficult to ascribe this peak to a vibronically allowed transition associated with the 1PA state, as it will be discussed below; we ascribe this state to an independent electronic state. The unsymmetrical compound **SD-2b** exhibited noticeably lower peak 2PA efficiency with a larger maximum at the vibrational shoulder of the main linear absorption band. Efficient 2PA properties of these new squaraines revealed their high potential for manifold two-photon applications.

3.7. Quantum Chemical Calculations. The optimized structures, frontier molecular orbitals, and the orbital contours of the HOMO and LUMO, calculated by DFT calculations, are shown in Figures 7, S2, and S3. In the central four-membered ring, the electronic distributions of HOMO orbitals are localized, while the LUMO orbitals are depleted. The energies of the dyes increase by 0.73 eV for LUMO and 0.96 eV for HOMO by changing the number of methoxyl groups, which can be related to their hypsochromic shifts in the absorption maxima. The nitrogen atoms in the dialkylamine groups become essentially conjugated with the benzene ring, mainly suggesting electron donation to the π system of the squaraines.[21] More importantly, the optimized geometry of **SD-0** is almost planar, in agreement with the values reported in the literature.[23,57] Distorted dihedral angles between the methoxy-related aniline unit and the four-membered squaraine core are summarized in Chart 1. The dihedral angle is calculated at ca. 11° in **SD-2a** and ca. 30° in **SD-4**. **SD-2b** has two different dihedral angles (ca. 28° and 1°) in order to minimize the steric repulsion, which gives limited delocalization
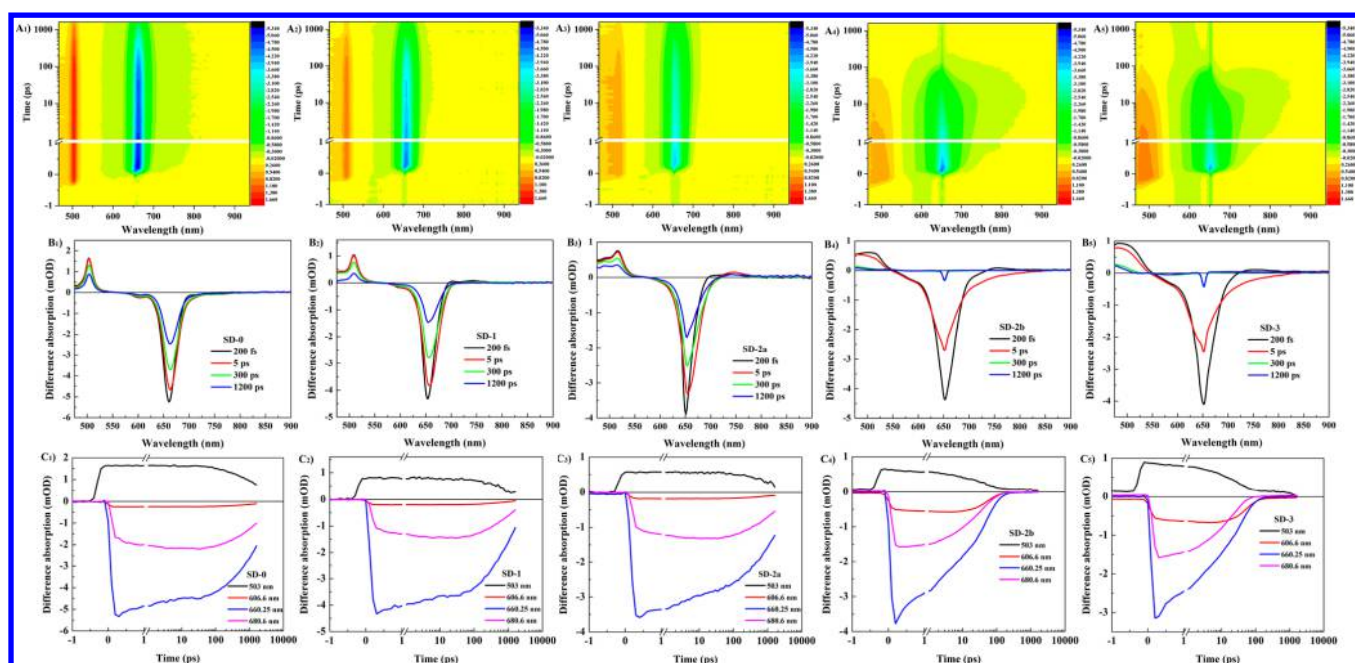
Figure 5. (A) Contour plots of the difference absorption signals, ΔD, as a function of time delay, τ_D, for **SD-0** (A_1), **SD-1** (A_2), **SD-2a** (A_3), **SD-2b** (A_4), and **SD-3** (A_5) in DCM (λ_{ex} = 650 nm). (B) Transient absorption spectra at selected delays, τ_D (see inserts), for **SD-0** (B_1), **SD-1** (B_2), **SD-2a** (B_3), **SD-2b** (B_4), and **SD-3** (B_5) in DCM. (C) Transient absorption dependences ($\Delta D = f(\tau_D)$) at selected wavelengths (see insets) for **SD-0** (C_1), **SD-1** (C_2), **SD-2a** (C_3), **SD-2b** (C_4), and **SD-3** (C_5) in DCM.
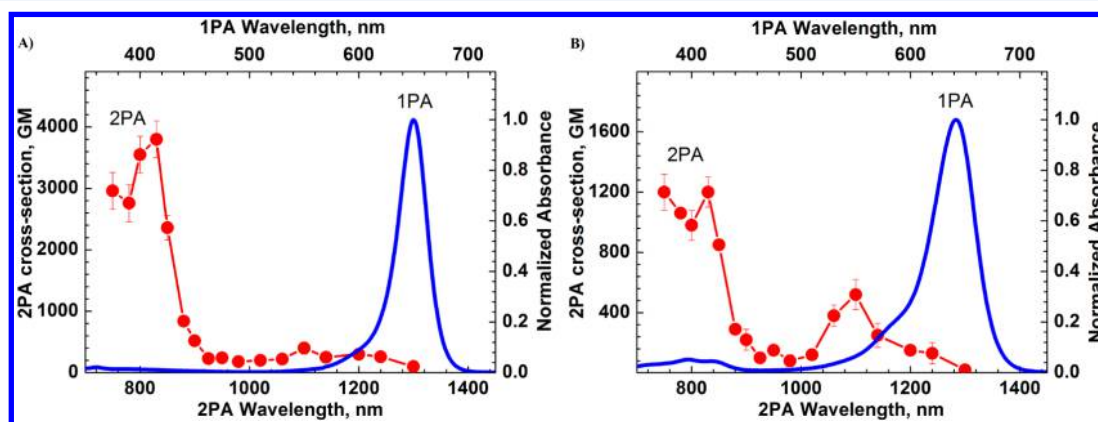
Figure 6. Degenerate 2PA spectra of **SD-2a** (A) and **SD-2b** (B) in DCM.
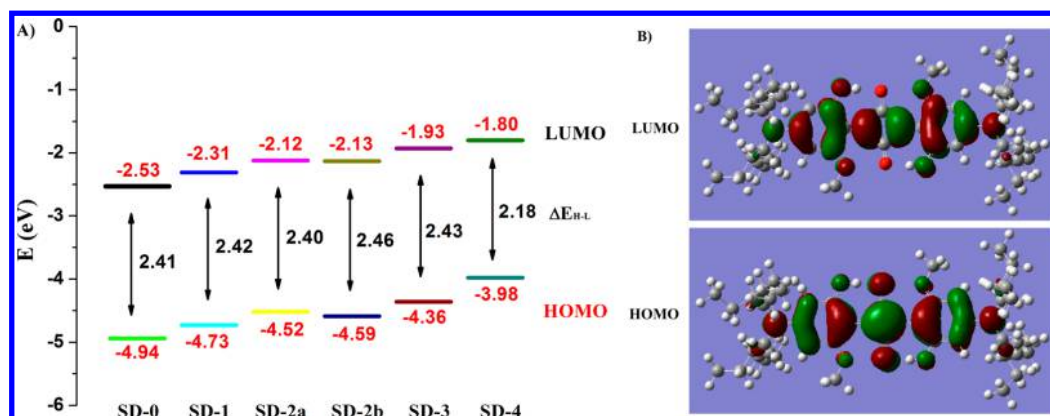
Figure 7. (A) HOMO and LUMO energies and theoretical energy gaps of the dyes calculated at the B3LYP/6-31G(d) level. (B) Molecular orbital contours of the HOMO and LUMO for **SD-2a**.
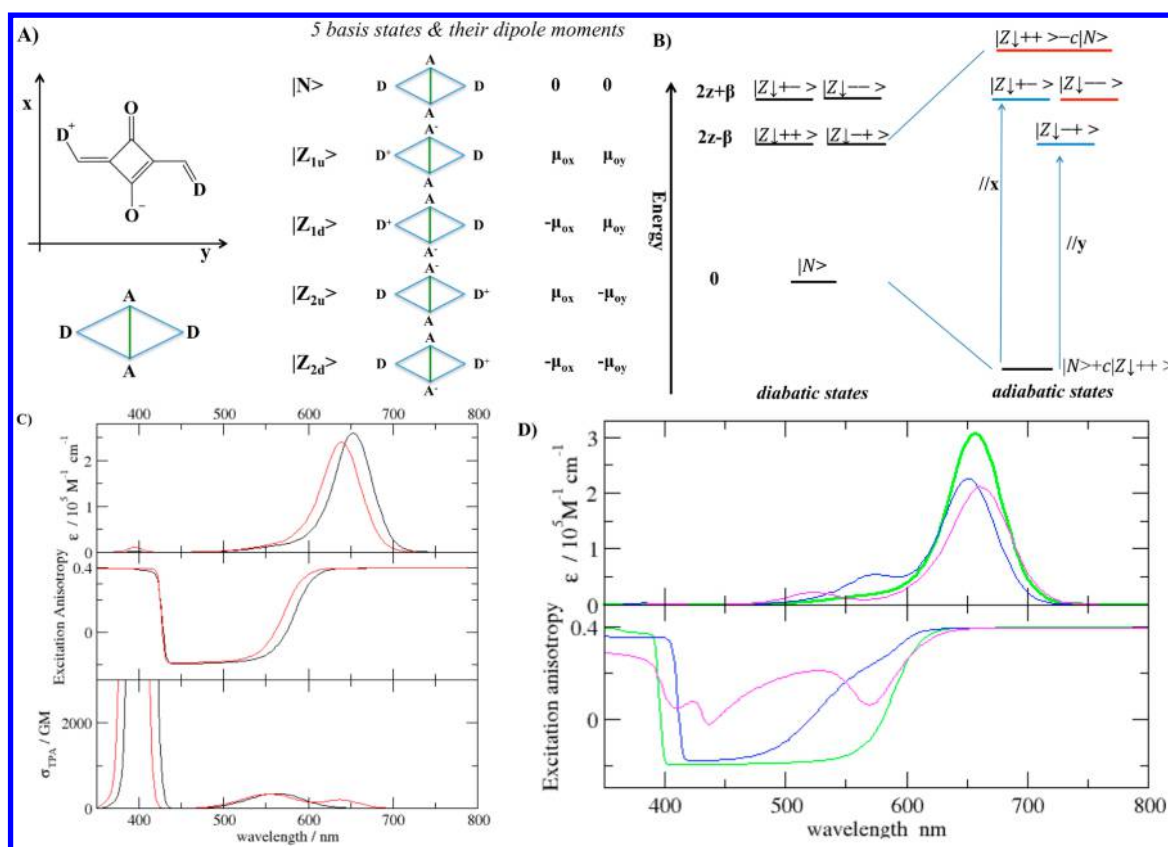
Figure 8. (A) Structure of a squaraine and its schematic representation. The 5 basis states and their dipole moment along x and y (all off-diagonal dipole moments are neglected). (B) The case of a symmetric squaraine. On the left the basis (adiabatic) states with corresponding energies; on the right the corresponding eigenstates (the adiabatic state). Blue and red colors refer to adiabatic states. (C) Calculated spectra for **SD-2a** and **SD-2b** dyes are reported as black and red lines, respectively. Top panel: linear absorption (continuous lines) and fluorescence spectra (dashed lines, arbitrary units). Middle panel: fluorescence anisotropy spectra (calculated for emission at 670 nm). Bottom panel: 2PA spectra. (D) Calculated spectra for **SD** family. Top panel: absorbance (continuous lines) and fluorescence spectra (dashed lines, arbitrary units). Bottom panel: fluorescence anisotropy calculated for emission at 670 nm. Black, red, green, blue, and magenta lines refer to **SD-2a**, **SD-2b**, **SD-0**, **SD-1**, and **SD-3**, respectively.

of the excited state.[58] We can see that the larger nonplanarity in the squaraine molecule led to a greater decrease in conjugation of the whole π system, resulting in a larger change of the photophysical properties in comparison with the original dye **SD-0**.[59] **SD-2a** is considered to assume an *anti*-conformation on the basis of preliminary calculations. In fact, after geometry optimizations, this conformation resulted to be energetically more stable than the corresponding *syn*-conformation. The strong effect of steric hindrance is also evident in optimized **SD-4**, and the larger angle can equally explain its poor stability and the difficulty in synthesis as discussed above.[21,23]

The calculated energy gaps (ΔE_{H-L}) and the optical energy gaps ($Eg_{expl.}$) are also shown in Table 1. The optical band gaps of these dyes, obtained from their UV−vis spectra, show a similar increasing trend in the range of 1.84−1.87 eV. This provided further evidence for the decrease of effective conjugation in the squaraine dye from **SD-1** to **SD-3**. The calculated energy gaps appear to be systematically higher than the optical band gaps, which is presumably because of the fact that the calculations were performed in vacuum.[60,61] According to the calculations and experimental data, the number and position of the substituent groups as well as distortion from planarity can influence the electronic delocalization and the photophysical properties of the dyes.

3.8. Essential State Models. The minimal model for squaraine dyes describes them as D-π−A−π-D or quadrupolar

dyes, where A represents the squaraic core that acts as an electron acceptor unit with respect to the lateral groups acting as electron donors.[62] The basic physics and low-energy spectroscopy of squaraine dyes is then explained in terms of three resonating structures: D-π−A−π-D ↔ D$^+$-π-A$^-$−π-D ↔ D$^-$-π−A−π-D$^+$. The three-state model accounts for the intense, narrow, and almost structureless 1PA band that characterizes squaraine spectra and the almost specular emission band with marginal Stokes shift. It also predicts a 2PA band located approximately at twice the energy of the linear absorption whose intensity is amplified by quasi-resonance effects.[62,63] Within the same model, squaraines are classified as class II quadrupolar dyes, a family of dyes that are not prone to symmetry breaking, that instead affects the lowest excited state of class I quadrupolar dyes and the ground state of class III dyes. The model was also extended to discuss asymmetric squaraines, explaining their anomalous solvatochromism.[64] However, there are a few features of the squaraine's spectra that cannot be accounted for in the three-state model.

The most obvious deviation from the predictions of the three-state model is the anisotropy dip observed in the spectral region comprised between the linear absorption band and the 2PA band,[65] pointing to the presence of an intermediate state with a polarization perpendicular to the main molecular axis. Dips in fluorescence anisotropy were also observed for cyanine dyes, usually located in the close proximity of the 2PA state.[65]

The flexible and definitely nonperfectly linear structure of cyanine dyes allows ascribing these dips to the 2PA states that, for slightly bent cyanines, is expected to be orthogonal to the main absorption band, polarized along the main molecular axis. This explanation does not apply to squaraine dyes, which are characterized by a rigid and symmetric structure. The only possibility to account for states polarized perpendicularly to the main molecular axis then requires one to account for the inner degrees of freedom of the squaric ring, observing that actually each squaric core provides two acceptor sites corresponding to the two oxygen atoms. Accordingly, a squaraine dye can be described as a D(A)$_2$D, whose main resonating structures are schematically shown in Figure 8A.

The relevant Hamiltonian, accounting for the electron hopping among D and A sites (τ-terms), as well as for the charge resonance along the x direction (β term), reads:

$$H_{el} = \begin{matrix} 0 & -\tau_{1u} & -\tau_{1d} & -\tau_{2u} & -\tau_{2d} \\ -\tau_{1u} & 2z_{1u} & -\beta & 0 & 0 \\ -\tau_{1d} & -\beta & 2z_{1d} & 0 & 0 \\ -\tau_{2u} & 0 & 0 & 2z_{2u} & -\beta \\ -\tau_{2d} & 0 & 0 & -\beta & 2z_{2d} \end{matrix} \tag{1}$$

where, to account for the most general case, we have assigned a different diagonal energy to the four zwitterionic states (the energy of the $|N\rangle$ state is set to zero) and a different hopping term for each state.

It is instructive to start the analysis with symmetric squaraines, like **SD-0** and **SD-2a**. In this case the four zwitterionic states are degenerate, and we set $z = z_{1u} + z_{1d} + z_{2u} + z_{2d}$ and $\tau = \tau_{1u} + \tau_{1d} + \tau_{2u} + \tau_{2d}$. We exploit the symmetry of the system and in particular the two C2 axes along the directions x and y to define the symmetrized basis states

$$|N\rangle$$

$$|Z_{++}\rangle = \frac{1}{2}(|Z_{1u}\rangle + |Z_{1d}\rangle + |Z_{2u}\rangle + |Z_{2d}\rangle)$$

$$|Z_{+-}\rangle = \frac{1}{2}(|Z_{1u}\rangle - |Z_{1d}\rangle + |Z_{2u}\rangle - |Z_{2d}\rangle)$$

$$|Z_{-+}\rangle = \frac{1}{2}(|Z_{1u}\rangle + |Z_{1d}\rangle - |Z_{2u}\rangle - |Z_{2d}\rangle)$$

$$|Z_{--}\rangle = \frac{1}{2}(|Z_{1u}\rangle - |Z_{1d}\rangle - |Z_{2u}\rangle + |Z_{2d}\rangle) \tag{2}$$

where the first and second subscripts in the symmetrized functions refer to the parity with respect to the y- and x-axis, respectively. As illustrated in Figure 8B, $|N\rangle$ and the totally symmetric state Z_{++} mix to give the ground state $|G\rangle$ and a totally symmetric excited state $|E\rangle$, which is forbidden in 1PA but 2PA allowed. The Z_{-+} state stays unmixed at energy $2z$-β and corresponds to a 1PA allowed with polarization along the long molecular axis (2PA forbidden) state. Finally, the two states Z_{+-} and Z_{--} stay unmixed at energy $2z$+β and are allowed in 1PA (x-polarization) and 2PA, respectively. Since the molecule is very elongated, we expect that $\mu x < \mu y$, or in other terms, we expect that optical spectra are mainly governed by transitions along the main molecular axis. As long as we are interested in the main spectral features, a three-state model accounting for N, Z$_{++}$, and Z$_{+-}$ states is enough and easily maps

into the three-state model originally proposed and successfully developed for squaraine dyes.[62]

In a more detailed analysis, the five-state model immediately suggests the presence of a 1PA state polarized perpendicularly to the main molecular axis located between the 1PA, then explaining the observation of dips in the fluorescence anisotropy spectra in the region between the main 1PA and 2PA band, due to the Z$_{-+}$ state. Indeed the model predicts the presence of a weak 2PA state, Z$_{--}$, degenerate with the Z$_{-+}$ state, responsible for the dip in the fluorescence anisotropy. We ascribe to this state the small 2PA peak to the red of the main 1PA band (at ∼550 and 560 nm for **SD-2a** and **SD-2b**, respectively, see Figure 3C). Of course this degeneracy is maintained only in the simple model, and a splitting between the two states is expected due to the interactions with other states not accounted for in this simplified picture.

In order to actually compare with experimental spectra and specifically to address line shapes, we introduce the coupling between electronic degrees of freedom and molecular vibrations. Following a similar strategy as with the three-state model,[62] we introduce two effective vibrations that account for the different geometry on the left and right molecular arm when charge transfer occurs on the specific arm. The Hamiltonian reads

$$\begin{aligned} H_{mol} = H_{el} &- \sqrt{\varepsilon_v}\,\omega_v Q_1(|Z_{1u}\rangle\langle Z_{1u}| + |Z_{1d}\rangle\langle Z_{1d}|) \\ &- \sqrt{\varepsilon_v}\,\omega_v Q_2(|Z_{2u}\rangle\langle Z_{2u}| + |Z_{2d}\rangle\langle Z_{2d}|) \\ &+ \frac{1}{2}[\omega_v^2(Q_1^2 + Q_2^2) + P_1^2 + P_2^2] \end{aligned} \tag{3}$$

where Q_1 and Q_2 are the two effective molecular coordinates associated with the two molecular arms; P_1 and P_2 are the conjugated momenta; and ω_v and ε_v are the vibrational frequencies and relaxation energy, assumed for simplicity equal for the two arms, even in asymmetric molecules. Finally, to reproduce the inhomogeneous broadening due to polar solvation, we introduce the coupling with the solvent in terms of the reaction field, F, as follows

$$H = H_{mol} - \vec{F}\cdot\vec{\mu} + \frac{F^2}{4\varepsilon_{or}} \tag{4}$$

where ε_{or} is the solvent relaxation energy that increases with solvent polarity. The Hamiltonian is solved as described in the Supporting Information.

We do not attempt to reproduce the small solvatochromism observed for the dyes. Indeed our model only accounts for nonspecific effects, while the presence of pH-sensitive groups in the squaraic core calls for specific effects. We set $\varepsilon_{or} = 0.1$ eV with reference to results in THF, as a mildly polar solvent, similar to pTHF used for fluorescence anisotropy spectra. Our aim is to obtain an overall picture of the physics of the family of squaraine dyes discussed in this work, offering a unifying interpretative scheme, which, in view of the simplicity of the model, can only capture their main spectroscopic features. We therefore fix as common model parameters for all dyes $\varepsilon_v = 0.1$ eV, $\omega_v = 0.12$ eV, $\mu_y = 24.0$ D, $\mu_x = 6.5$ D, and $\gamma = 0.07$ eV. The first two parameters account for the vibronic shape of the linear absorption spectrum; μ_y and μ_x are fixed to reproduce the spectral intensity; and γ is the width assigned to each vibronic line (see Supporting Information). The parameter β, responsible for the charge resonance between the two oxygens across the squaraine core, is fixed with reference to the spectra

of symmetric dyes (**SD-2a** and **SD-0**) where 2β measures the energy gap between the main 1PA state (Z_{-+}) and the two degenerate Z_{+-} and Z_{--}, responsible for the anisotropy dip and for the weak 2PA band, respectively (cf. Figure 8B).

Accordingly we fix β = 0.15 eV, based on **SD-2a** spectra, and maintain the same value for all dyes. We start our analysis from **SD-2a** and **SD-2b**, where both 1PA and 2PA spectra are available. For **SD-2a** we best reproduce the spectra fixing $2z$ = 0.48 eV and τ = 0.74 eV (see Table 3). Moving to **SD-2b**, we

Table 3. Primary Model Parameters (eV Units) for the SD Dyes

	SD-2a	SD-2b	SD-0	SD-1	SD-3
$z1u = z2u$	0.48	0.48	0.32	0.48	0.68
$z1d = z2d$				0.32	0.48
$\tau 1u = \tau 1d$	0.74	0.83	0.83	0.74	0.68
$\tau 2u = \tau 2d$		0.68			0.74

expect (to the first approximation) unchanged $2z$ since the local environment of the squaraine-core oxygens is the same in the two dyes. However, based on the DFT geometries (see Figures 7, S2, and S3), we do expect different τ for the left and right arms. Best fit to experimental data is obtained with the τ values listed in Table 3. Calculated spectra for **SD-2a** and **SD-2b** are reported in Figure 8C.

Linear absorption spectra of **SD-2a** and **SD-2b** are well reproduced, with a blue shift and a slight decrease of intensity when going from the symmetric **SD-2a** to the asymmetric **SD-2b** dye. 2PA spectra reproduce fairly accurately the experimental data, with a band at ~560 nm ascribed to the Z_{--} state and a secondary band at ~650 nm related to a vibronically allowed contribution from the 1PA state. As for the high frequency region, we reproduce the main 2PA band, which, due to preresonant enhancement, has large 2PA intensity.

However, experimental spectra show an additional structure on the shoulder of the 2PA band. This structure points to the presence of additional states, not included in our model. Additional data, and specifically excited-state absorption spectra, would be needed to precisely parametrize the relevant states, as was done to explain similar structures in the 2PA band of cyanine dyes.[66] The main success of our 5-state model concerns the inclusion of a state with polarization perpendicular to the main molecular axis, then explaining the puzzling observation of a dip in the fluorescence anisotropy spectra of squaraine dyes. In cyanine dyes a dip in anisotropy is always observed at frequencies corresponding to the main 2PA band and can be therefore ascribed to the slightly bent quadrupolar structure of the cyanine skeleton.[65] However, in squaraines, the dip is located somewhere between the main 1PA and 2PA bands, and in view of the rigid and strictly linear molecular structure of squaraine dyes, it calls for a different origin. Our results suggest it can be ascribed to the presence of a charge resonance across the squaraine core. Indeed the dip we calculate is red-shifted with respect to the experiment, and it is too wide. Both features could be improved, accounting for additional states, as already discussed with reference to 2PA spectra. Indeed it is very clear that, while the proposed 5-state model is an improvement over the basic 3-state model for squaraines, additional states are required to address 2PA spectra, as well as to remove the degeneracy of the Z_{-+} and Z_{--}

states moving the Z_{-+} state, responsible for the dip at higher energy with respect to the Z_{--} state.

We can now transfer the information to build the model for other dyes: for **SD-0**, we take the same τ as for the flat arm of **SD-2b** but decrease $2z$ to account for the decreased energy of zwitterionic states related to the stronger electron-accepting character of the squaraic oxygen when involved in two hydrogen bonds, with respect to a single hydrogen bond, as for **SD-2a** and **SD-2b** dyes. Along similar lines we define the model parameters for **SD-1** and **SD-3**, as listed in Table 3. Calculated spectra are shown in Figure 8D (calculated fluorescence spectra are reported in the Supporting Information) and compare favorably with experimental results, suggesting that the proposed model captures the main physics of this family of squaraine dyes.

4. CONCLUSIONS

In summary, we prepared and characterized a series of novel squaraine dyes to serve as a basis to understand molecular design and photophysical properties in an important class of organic photonic materials. These dyes show favorable absorption and emission suitable for potential NIR optical applications such as imaging and photovoltaics. The numbers and positions of methyl substituents affect the LUMO and HOMO energy levels of the related squaraine dyes in discrete manners. Meanwhile, the substituents also impact aggregation behavior in DMSO/H$_2$O solutions. For example, **SD-2a** was not prone to aggregation, a process that plagues many similar molecules in polar media, and maintained high fluorescence quantum yield. On the other hand, the low quantum yields and fluorescence lifetimes of **SD-2b** and **SD-3** revealed the pronounced effect of rather subtle changes in structure, i.e., arrangement and number of methyl substituents, on the optical properties of this series of squaraine dyes. Comprehensive photophysical studies were complemented with theoretical computations and analysis. We found that there was reasonable qualitative agreement between experimental and calculated results using a five-state model. Transient absorption spectral investigations elucidated fast temporal processes, such as excited state absorption, saturable absorption, and gain that were dependent on the number and position of methyl substitution. Additionally, two of the squaraine dyes exhibited large two-photon absorption. This systematic study helps to clarify the parameters by which squaraine dyes, especially dihydroxylaniline-based squaraine dyes, may be fine-tuned for particular purposes and provides a better understanding of the relationship between structural and optical properties that may be valuable in developing new or improved near-IR absorbing chromophores for solar cells and biological imaging.

■ ASSOCIATED CONTENT

Ⓢ Supporting Information

The Supporting Information is available free of charge on the ACS Publications website at DOI: 10.1021/acs.jpcc.7b11997. Crystallographic data of **SD-2a** are available from the Cambridge Crystallographic Data Centre as publication nos. CCDC- 1537057. Copies of the data can be obtained free of charge on application to CCDC via the Internet at http://www. ccdc.cam.ac.uk.

Detailed synthetic procedures and characterization data for new intermediates, theoretical calculation details are

provided as well as detailed crystallographic information for **SD-2a** (PDF)

AUTHOR INFORMATION

Corresponding Author
*E-mail: belfield@njit.edu. Tel.: 1-973-596-3676.

ORCID
Taihong Liu: 0000-0002-9600-1045
Xinglei Liu: 0000-0002-1457-9928
Shengli Zou: 0000-0003-1302-133X
Anna Painelli: 0000-0002-3500-3848
Yuanwei Zhang: 0000-0003-2111-0981
Yu Fang: 0000-0001-8490-8080
Kevin D. Belfield: 0000-0002-7339-2813

Notes
The authors declare no competing financial interest.

REFERENCES

(1) Jiang, P.; Tian, Z. Q.; Zhu, C. N.; Zhang, Z. L.; Pang, D. W. Emission-Tunable Near-Infrared Ag_2S Quantum Dots. *Chem. Mater.* **2012**, *24*, 3−5.

(2) Ren, L.; Liu, F.; Shen, X.; Zhang, C.; Yi, Y.; Zhu, X. Developing Quinoidal Fluorophores with Unusually Strong Red/Near-Infrared Emission. *J. Am. Chem. Soc.* **2015**, *137*, 11294−11302.

(3) Wu, I. C.; Yu, J.; Ye, F.; Rong, Y.; Gallina, M. E.; Fujimoto, B. S.; Zhang, Y.; Chan, Y. H.; Sun, W.; Zhou, X. H.; Wu, C.; Chiu, D. T. Squaraine-Based Polymer Dots with Narrow, Bright Near-Infrared Fluorescence for Biological Applications. *J. Am. Chem. Soc.* **2015**, *137*, 173−178.

(4) Tchounwou, C.; Sinha, S. S.; Viraka Nellore, B. P.; Pramanik, A.; Kanchanapally, R.; Jones, S.; Chavva, S. R.; Ray, P. C. Hybrid Theranostic Platform for Second Near-IR Window Light Triggered Selective Two-Photon Imaging and Photothermal Killing of Targeted Melanoma Cells. *ACS Appl. Mater. Interfaces* **2015**, *7*, 20649−20656.

(5) Bwambok, D. K.; El-Zahab, B.; Challa, S. K.; Li, M.; Chandler, L.; Baker, G. A.; Warner, I. M. Near-Infrared Fluorescent NanoGUMBOS for Biomedical Imaging. *ACS Nano* **2009**, *3*, 3854−3860.

(6) Yuan, L.; Lin, W.; Yang, Y.; Chen, H. A Unique Class of Near-Infrared Functional Fluorescent Dyes with Carboxylic-Acid-Modulated Fluorescence ON/OFF Switching: Rational Design, Synthesis, Optical Properties, Theoretical Calculations, and Applications for Fluorescence Imaging in Living Animals. *J. Am. Chem. Soc.* **2012**, *134*, 1200−1211.

(7) Oguz, U.; Akkaya, E. U. One-Pot Synthesis of Squaraine Fluoroionophores. *J. Org. Chem.* **1998**, *63*, 6059−6060.

(8) Goh, T.; Huang, J. S.; Bielinski, E. A.; Thompson, B. A.; Tomasulo, S.; Lee, M. L.; Sfeir, M. Y.; Hazari, N.; Taylor, A. D. Coevaporated Bisquaraine Inverted Solar Cells: Enhancement Due to Energy Transfer and Open Circuit Voltage Control. *ACS Photonics* **2015**, *2*, 86−95.

(9) Yang, D.; Zhu, Y.; Jiao, Y.; Yang, L.; Yang, Q.; Luo, Q.; Pu, X.; Huang, Y.; Zhao, S.; Lu, Z. N,N-Diarylamino End-Capping as a New Strategy for Simultaneously Enhancing Open-Circuit Voltage, Short-Circuit Current Density and Fill Factor in Small Molecule Organic Solar Cells. *RSC Adv.* **2015**, *5*, 20724−20733.

(10) Maeda, T.; Nitta, S.; Nakao, H.; Yagi, S.; Nakazumi, H. Squaraine Dyes with Pyrylium and Thiopyrylium Components for Harvest of Near Infrared Light in Dye-Sensitized Solar Cells. *J. Phys. Chem. C* **2014**, *118*, 16618−16625.

(11) Corredor, C. C.; Huang, Z. L.; Belfield, K. D. Two-Photon 3D Optical Data Storage via Fluorescence Modulation of an Efficient Fluorene Dye by a Photochromic Diarylethene. *Adv. Mater.* **2006**, *18*, 2910−2914.

(12) Emmelius, M.; Pawlowski, G.; Vollmann, H. W. Materials for Optical Data Storage. *Angew. Chem., Int. Ed. Engl.* **1989**, *28*, 1445−1471.

(13) Jipson, V. B.; Jones, C. R. Infrared Dyes for Optical Storage. *J. Vac. Sci. Technol.* **1981**, *18*, 105−109.

(14) Zhang, Y.; Kim, B.; Yao, S.; Bondar, M. V.; Belfield, K. D. Controlled Aggregation and Enhanced Two-Photon Absorption of a Water-Soluble Squaraine Dye with a Poly(acrylic acid) Template. *Langmuir* **2013**, *29*, 11005−11012.

(15) Sun, C. L.; Liao, Q.; Li, T.; Li, J.; Jiang, J. Q.; Xu, Z. Z.; Wang, X. D.; Shen, R.; Bai, D. C.; Wang, Q.; et al. Rational Design of Small Indolic Squaraine Dyes with Large Two-Photon Absorption Cross Section. *Chem. Sci.* **2015**, *6*, 761−769.

(16) Lee, S.; Rao, B. A.; Son, Y. A. A Highly Selective Fluorescent Chemosensor for Hg^{2+} Based on a Squaraine-Bis(Rhodamine-B) Derivative: Part II. *Sens. Sens. Actuators, B* **2015**, *210*, 519−532.

(17) Ajayaghosh, A. Chemistry of Squaraine-Derived Materials: Near-IR Dyes, Low Band Gap Systems, and Cation Sensors. *Acc. Chem. Res.* **2005**, *38*, 449−459.

(18) Karpenko, I. A.; Klymchenko, A. S.; Gioria, S.; Kreder, R.; Shulov, I.; Villa, P.; Mely, Y.; Hibert, M.; Bonnet, D. Squaraine as a Bright, Stable and Environment-Sensitive Far-Red Label for Receptor-Specific Cellular Imaging. *Chem. Commun.* **2015**, *51*, 2960−2963.

(19) Luo, C.; Zhou, Q.; Jiang, G.; He, L.; Zhang, B.; Wang, X. The Synthesis and $^1O_2$ Photosensitization of Halogenated Asymmetric Aniline-Based Squaraines. *New J. Chem.* **2011**, *35*, 1128−1132.

(20) Kurhuzenkau, S. A.; Woodward, A. W.; Yao, S.; Belfield, K. D.; Shaydyuk, Y. O.; Sissa, C.; Bondar, M. V.; Painelli, A. Ultrafast Spectroscopy, Superluminescence and Theoretical Modeling of a Two-Photon Absorbing Fluorene Derivative. *Phys. Chem. Chem. Phys.* **2016**, *18*, 12839−12846.

(21) Wang, S.; Hall, L.; Diev, V. V.; Haiges, R.; Wei, G.; Xiao, X.; Djurovich, P. I.; Forrest, S. R.; Thompson, M. E. N,N-Diarylanilinosquaraines and Their Application to Organic Photovoltaics. *Chem. Mater.* **2011**, *23*, 4789−4798.

(22) Chen, H.; Farahat, M. S.; Law, K. Y.; Whitten, D. G. Aggregation of Surfactant Squaraine Dyes in Aqueous Solution and Microheterogeneous Media: Correlation of Aggregation Behavior with Molecular Structure. *J. Am. Chem. Soc.* **1996**, *118*, 2584−2594.

(23) Bruck, S.; Krause, C.; Turrisi, R.; Beverina, L.; Wilken, S.; Saak, W.; Lutzen, A.; Borchert, H.; Schiek, M.; Parisi, J. Structure-Property Relationship of Anilino-Squaraines in Organic Solar Cells. *Phys. Chem. Chem. Phys.* **2014**, *16*, 1067−1077.

(24) Tian, M.; Furuki, M.; Iwasa, I.; Sato, Y.; Pu, L. S.; Tatsuura, S. Search for Squaraine Derivatives That Can Be Sublimed without Thermal Decomposition. *J. Phys. Chem. B* **2002**, *106*, 4370−4376.

(25) Chen, G.; Sasabe, H.; Sasaki, Y.; Katagiri, H.; Wang, X. F.; Sano, T.; Hong, Z.; Yang, Y.; Kido, J. A Series of Squaraine Dyes: Effects of Side Chain and the Number of Hydroxyl Groups on Material Properties and Photovoltaic Performance. *Chem. Mater.* **2014**, *26*, 1356−1364.

(26) Law, K. Y. Squaraine Chemistry: Effects of Structural Changes on the Absorption and Multiple Fluorescence Emission of Bis[4-(dimethylamino)phenyl]squaraine and Its Derivatives. *J. Phys. Chem.* **1987**, *91*, 5184−5193.

(27) Liu, X. D.; Sun, R.; Ge, J. F.; Xu, Y. J.; Xu, Y.; Lu, J. M. A Squaraine-Based Red Emission Off-On Chemosensor for Biothiols and

Its Application in Living Cells Imaging. *Org. Biomol. Chem.* **2013**, *11*, 4258−4264.

(28) *APEX2 (2009.11−0). Program for Bruker CCD X-ray Diffractometer Control*; Bruker AXS Inc.: Madison, WI, USA, 2009.

(29) Sheldrick, G. M. SHELXT-Integrated Space-Group and Crystal-Structure Determination. *Acta Crystallogr., Sect. A: Found. Adv.* **2015**, *71*, 3−8.

(30) Sheldrick, G. M. Crystal Structure Refinement with SHELXL. *Acta Crystallogr., Sect. C: Struct. Chem.* **2015**, *71*, 3−8.

(31) Dolomanov, O. V.; Bourhis, L. J.; Gildea, R. J.; Howard, J. A. K.; Puschmann, H. OLEX2: A Complete Structure Solution, Refinement and Analysis Program. *J. Appl. Crystallogr.* **2009**, *42* (2), 339−341.

(32) Emsley, P.; Cowtan, K. Coot: Model-Building Tools for Molecular Graphics. *Acta Crystallogr., Sect. D: Biol. Crystallogr.* **2004**, *60*, 2126−2132.

(33) Barkauskas, M.; Martynaitis, V.; Šačkus, A.; Rotomskis, R.; Sirutkaitis, V.; Vengris, M. Ultrafast Dynamics of Photochromic Compound Based on Oxazine Ring Opening. *Lith. J. Phys.* **2008**, *48*, 231−242.

(34) Redeckas, K.; Voiciuk, V.; Steponavičiūtė, R.; Martynaitis, V.; Šačkus, A.; Vengris, M. Ultrafast Spectral Dynamics of Structurally Modified Photochromic Indolo[2,1-*b*][1,3]benzoxazines. *J. Photochem. Photobiol., A* **2014**, *285*, 7−15.

(35) Sheik-Bahae, M.; Said, A. A.; Wei, T. H.; Hagan, D. J.; Van Stryland, E. W. Sensitive Measurement of Optical Nonlinearities Using a Single Beam. *IEEE J. Quantum Electron.* **1990**, *26*, 760−769.

(36) Ajayaghosh, A.; Chithra, P.; Varghese, R. Self-Assembly of Tripodal Squaraines: Cation-Assisted Expression of Molecular Chirality and Change from Spherical to Helical Morphology. *Angew. Chem., Int. Ed.* **2007**, *46*, 230−233.

(37) Hu, L.; Yan, Z.; Xu, H. Advances in Synthesis and Application of Near-Infrared Absorbing Squaraine Dyes. *RSC Adv.* **2013**, *3*, 7667−7676.

(38) Law, K. Y. Squaraine Chemistry. Absorption, Fluorescence Emission, and Photophysics of Unsymmetrical Squaraines. *J. Phys. Chem.* **1995**, *99*, 9818−9824.

(39) Chen, C. T.; Marder, S. R.; Cheng, L. T. Syntheses and Linear and Nonlinear Optical Properties of Unsymmetrical Squaraines with Extended Conjugation. *J. Am. Chem. Soc.* **1994**, *116*, 3117−3118.

(40) Kazmaier, P. M.; Hamera, G. K.; Burt, R. A. Conformational Isomerism in Squaraines: Saturation Transfer NMR Studies on Hydroxy Squaraines. *Can. J. Chem.* **1990**, *68*, 530−536.

(41) Tong, L.; Bi-Xian, P.; Fenglian, B. The Structure and ^{13}C-NMR of an Indolenium Squaraine Dye. *Dyes Pigm.* **1999**, *43*, 67−71.

(42) Yang, L.; Zhu, Y.; Jiao, Y.; Yang, D.; Chen, Y.; Wu, J.; Lu, Z.; Zhao, S.; Pu, X.; Huang, Y. The Influence of Intramolecular Noncovalent Interactions in Unsymmetrical Squaraines on Material Properties, Film Morphology and Photovoltaic Performance. *Dyes Pigm.* **2017**, *145*, 222−232.

(43) Ajayaghosh, A.; Arunkumar, E. ^{1}H NMR Spectral Evidence for a Specific Host-Guest Complexation Induced Charge Localization in Squaraine Dyes. *Org. Lett.* **2005**, *7*, 3135−3138.

(44) Dirk, C. W.; Herndon, W. C.; Cervantes-Lee, F.; Selnau, H.; Martinez, S.; Kalamegham, P.; Tan, A.; Campos, G.; Velex, M. Squarylium Dyes: Structural Factors Pertaining to the Negative Third-Order Nonlinear Optical Response. *J. Am. Chem. Soc.* **1995**, *117*, 2214−2225.

(45) Karpenko, I. A.; Collot, M.; Richert, L.; Valencia, C.; Villa, P.; Mely, Y.; Hibert, M.; Bonnet, D.; Klymchenko, A. S. Fluorogenic Squaraine Dimers with Polarity-Sensitive Folding as Bright Far-Red Probes for Background-Free Bioimaging. *J. Am. Chem. Soc.* **2015**, *137*, 405−412.

(46) Hestand, N. J.; Zheng, C.; Penmetcha, A. R.; Cona, B.; Cody, J. A.; Spano, F. C.; Collison, C. J. Confirmation of the Origins of Panchromatic Spectra in Squaraine Thin Films Targeted for Organic Photovoltaic Devices. *J. Phys. Chem. C* **2015**, *119*, 18964−18974.

(47) Ros-Lis, J. V.; Martinez-Manez, R.; Soto, J.; Villaescusa, L. A.; Rurack, K. Squaraine "Ships" in the Y Zeolite "Bottle": A Chromogenic Sensing Material for the Detection of Volatile Amines and Thiols. *J. Mater. Chem.* **2011**, *21*, 5004−5010.

(48) Belfield, K. D.; Andrade, C. D.; Yanez, C. O.; Bondar, M. V.; Hernandez, F. E.; Przhonska, O. V. New Two-Photon-Absorbing Probe with Efficient Superfluorescent Properties. *J. Phys. Chem. B* **2010**, *114*, 14087−14095.

(49) Toro, C.; Boni, L. D.; Yao, S.; Ritchie, J. P.; Masunov, A. E.; Belfield, K. B.; Hernandez, F. E. Linear and Nonlinear Optical Characterizations of a Monomeric Symmetric Squaraine-Based Dye in Solution. *J. Chem. Phys.* **2009**, *130*, 214504.

(50) Stoll, R. S.; Severin, N.; Rabe, J. P.; Hecht, S. Synthesis of a Novel Chiral Squaraine Dye and Its Unique Aggregation Behavior in Solution and in Self-Assembled Monolayers. *Adv. Mater.* **2006**, *18*, 1271−1275.

(51) Belfield, K. D.; Bondar, M. V.; Haniff, H. S.; Mikhailov, I. A.; Luchita, G.; Przhonska, O. V. Superfluorescent Squaraine with Efficient Two-Photon Absorption and High Photostability. *ChemPhysChem* **2013**, *14*, 3532−3542.

(52) Webster, S.; Peceli, D.; Hu, H.; Padilha, L. A.; Przhonska, O. V.; Masunov, A. E.; Gerasov, A. O.; Kachkovski, A. D.; Slominsky, Y. L.; Tolmachev, A. I.; et al. Near-Unity Quantum Yields for Intersystem Crossing and Singlet Oxygen Generation in Polymethine-Like Molecules: Design and Experimental Realization. *J. Phys. Chem. Lett.* **2010**, *1*, 2354−2360.

(53) Horng, M. L.; Gardecki, J. A.; Papazyan, A.; Maroncelli, M. Subpicosecond Measurements of Polar Solvation Dynamics: Coumarin 153 Revisited. *J. Phys. Chem.* **1995**, *99*, 17311−17337.

(54) Liu, T.; Bondar, M. V.; Belfield, K. D.; Anderson, D.; Masunov, A. E.; Hagan, D. J.; Stryland, E. W. V. Linear Photophysics and Femtosecond Nonlinear Spectroscopy of a Star-Shaped Squaraine Derivative with Efficient Two-Photon Absorption. *J. Phys. Chem. C* **2016**, *120*, 11099−11110.

(55) Odom, S. A.; Webster, S.; Padilha, L. A.; Peceli, D.; Hu, H.; Nootz, G.; Chung, S. J.; Ohira, S.; Matichak, J. D.; Przhonska, O. V.; et al. Synthesis and Two-Photon Spectrum of a Bis(Porphyrin)-Substituted Squaraine. *J. Am. Chem. Soc.* **2009**, *131*, 7510−7511.

(56) Fu, J.; Padilha, L. A.; Hagan, D. J.; Van Stryland, E. W.; Przhonska, O. V.; Bondar, M. V.; Slominsky, Y. L.; Kachkovski, A. D. Experimental and Theoretical Approaches to Understanding Two-Photon Absorption Spectra in Polymethine and Squaraine Molecules. *J. Opt. Soc. Am. B* **2007**, *24*, 67−76.

(57) Della Pelle, A. M.; Homnick, P. J.; Bae, Y.; Lahti, P. M.; Thayumanavan, S. Effect of Substituents on Optical Properties and Charge-Carrier Polarity of Squaraine Dyes. *J. Phys. Chem. C* **2014**, *118*, 1793−1799.

(58) Yang, D.; Yang, L.; Huang, Y.; Jiao, Y.; Igarashi, T.; Chen, Y.; Lu, Z.; Pu, X.; Sasabe, H.; Kido, J. Asymmetrical Squaraines Bearing Fluorine-Substituted Indoline Moieties for High-Performance Solution-Processed Small-Molecule Organic Solar Cells. *ACS Appl. Mater. Interfaces* **2015**, *7*, 13675−13684.

(59) Kim, J.; Kwon, Y. S.; Shin, W. S.; Moon, S. J.; Park, T. Carbazole-Based Copolymers: Effects of Conjugation Breaks and Steric Hindrance. *Macromolecules* **2011**, *44*, 1909−1919.

(60) Liu, T.; Ding, L.; He, G.; Yang, Y.; Wang, W.; Fang, Y. Photochemical Stabilization of Terthiophene and Its Utilization as a New Sensing Element in the Fabrication of Monolayer-Chemistry-Based Fluorescent Sensing Films. *ACS Appl. Mater. Interfaces* **2011**, *3*, 1245−1253.

(61) Liu, T.; Zhao, K.; Liu, K.; Ding, L.; Yin, S.; Fang, Y. Synthesis, Optical Properties and Explosive Sensing Performances of a Series of Novel *π*-Conjugated Aromatic End-Capped Oligothiophenes. *J. Hazard. Mater.* **2013**, *246−247*, 52−60.

(62) Terenziani, F.; Painelli, A.; Katan, C.; Charlot, M.; Blanchard-Desce, M. Charge Instability in Quadrupolar Chromophores: Symmetry Breaking and Solvatochromism. *J. Am. Chem. Soc.* **2006**, *128*, 15742−15755.

(63) Sissa, C.; Terenziani, F.; Painelli, A.; Bhaskar Kanth Siram, R.; Patil, S. Spectroscopic Characterization and Modeling of Quadrupolar

Charge-Transfer Dyes with Bulky Substituents. *J. Phys. Chem. B* **2012**, *116*, 4959−4966.

(64) Shafeekh, K. M.; Das, S.; Sissa, C.; Painelli, A. Asymmetric Squaraine Dyes: Spectroscopic and Theoretical Investigation. *J. Phys. Chem. B* **2013**, *117*, 8536−8546.

(65) Fu, J.; Padilha, L. A.; Hagan, D. J.; Van Stryland, E. W.; Przhonska, O. V.; Bondar, M. V.; Slominsky, Y. L.; Kachkovski, A. D. Experimental and Theoretical Approaches to Understanding Two-Photon Absorption Spectra in Polymethine and Squaraine Molecules. *J. Opt. Soc. Am. B* **2007**, *24*, 67−76.

(66) Sissa, C.; Mohamadzadeh Jahani, P.; Soos, Z. G.; Painelli, A. Essential State Model for Two-Photon Absorption Spectra of Polymethine Dyes. *ChemPhysChem* **2012**, *13*, 2795−2800.